

Error field penetration in J-TEXT tokamak based on two-fluid drift-MHD model

Wen Wang(王文), Tao Xu(徐涛), Yi Zhang(张仪), and the J-TEXT team

Citation: Chin. Phys. B, 2024, 33 (**4**): 045202. DOI: 10.1088/1674-1056/ad1e6b
Journal homepage: http://cpb.iphy.ac.cn; http://iopscience.iop.org/cpb

What follows is a list of articles you may be interested in

Magnetic diagnostics layout design for CFETR plasma equilibrium reconstruction

Qingze Yu(于庆泽), Yao Huang(黄耀), Zhengping Luo(罗正平), Yuehang Wang(汪悦航), Zijie Liu(刘自结), Wangyi Rui(芮望颐), Kai Wu(吴凯), Bingjia Xiao(肖炳甲), and Jiangang Li(李建刚)
Chin. Phys. B, 2024, 33 (**4**): 045201. DOI: 10.1088/1674-1056/ad23d6

Numerical study of alpha particle loss with toroidal field ripple based on CFETR steady-state scenario

Niuqi Li(李钮琦), Yingfeng Xu(徐颖峰), Fangchuan Zhong(钟方川), and Debing Zhang(张德兵)
Chin. Phys. B, 2024, 33 (**1**): 015202. DOI: 10.1088/1674-1056/ad03de

Stability impacts from the current and pressure profile modifications within finite sized island

Yuxiang Sun(孙宇翔) and Di Hu(胡地)
Chin. Phys. B, 2023, 32 (**7**): 075212. DOI: 10.1088/1674-1056/acd369

Drift surface solver for runaway electron current dominant equilibria during the current quench

Lu Yuan(袁露) and Di Hu(胡地)
Chin. Phys. B, 2023, 32 (**7**): 075208. DOI: 10.1088/1674-1056/acc1d7

Parametric decay instabilities of lower hybrid waves on CFETR

Taotao Zhou(周涛涛), Nong Xiang(项农), Chunyun Gan(甘春芸), Guozhang Jia(贾国章), and Jiale Chen(陈佳乐)
Chin. Phys. B, 2022, 31 (**9**): 095201. DOI: 10.1088/1674-1056/ac67c2

Error field penetration in J-TEXT tokamak based on two-fluid drift-MHD model

Wen Wang(王文), Tao Xu(徐涛)†, Yi Zhang(张仪), and the J-TEXT team

State Key Laboratory of Advanced Electromagnetic Technology,
International Joint Research Laboratory of Magnetic Confinement Fusion and Plasma Physics,
School of Electrical and Electronic Engineering, Huazhong University of Science and Technology, Wuhan 430074, *China*

(Received 28 November 2023; revised manuscript received 27 December 2023; accepted manuscript online 15 January 2024)

An externally generated resonant magnetic perturbation can induce complex non-ideal MHD responses in their resonant surfaces. We have studied the plasma responses using Fitzpatrick's improved two-fluid model and program LAYER. We calculated the error field penetration threshold for J-TEXT. In addition, we find that the island width increases slightly as the error field amplitude increases when the error field amplitude is below the critical penetration value. However, the island width suddenly jumps to a large value because the shielding effect of the plasma against the error field disappears after the penetration. By scanning the natural mode frequency, we find that the shielding effect of the plasma decreases as the natural mode frequency decreases. Finally, we obtain the $m/n = 2/1$ penetration threshold scaling on density and temperature.

Keywords: plasma responses, drift-MHD model, error field penetration

PACS: 52.55.Fa, 52.65.–y, 52.35.Py, 52.30.Cv **DOI:** 10.1088/1674-1056/ad1e6b

1. Introduction

Tearing mode is one of the magneto-hydrodynamic instabilities that greatly endanger the stable operation of tokamak. Error field (EF) generated by field-coil misalignments and non-axisymmetric coil feeds is responsible for the reconnection of magnetic lines.[1–3] For an intrinsically tearing-stable plasma, the error field can drive the growth of tearing modes. Fortunately, the reconnection of magnetic lines is significantly suppressed by the mode rotation in a tokamak plasma. Nevertheless, once the strength of the error field increases above a certain value, the mode rotation is suddenly arrested and thus leads to the unhindered expedition of magnetic reconnection. This is also called field penetration.[4–6] A series of experiments on error field penetration were performed on J-TEXT.[7–9] Moreover, a non-monotonic dependence on density is observed in J-TEXT.[8,10,11] The penetration threshold is in the range of $b_r/B_z \propto 10^{-4}$–10^{-3}. Here, b_r is the resonant harmonic of the radial EF, and B_z is the toroidal magnetic field. The scaling has been roughly derived in the form of $b_r/B_z \propto n_e^{\alpha_n} B_z^{\alpha_B} R_0^{\alpha_R}$, Here, n_e is the density, R_0 is the major radius, α_n, α_B, and α_R are the scaling coefficients on these parameters. $\alpha_n \sim 1$ in the nonlinear regime of error field penetration was proposed in the two-fluid model.[12] $\alpha_n \sim 1$ is observed in DIII-D,[6] TEXTOR,[13] and MAST,[14] while $\alpha_n \sim 0.5$ is observed in NSTX,[15] J-TEXT,[9] and EAST.[16] $\alpha_n \sim 0.5$ scaling in the linear regime is due to the predominant effect of poloidal ion fluid shift to the change in $\boldsymbol{E} \times \boldsymbol{B}$ frequency at the resonant surface.[17]

The linear inner region response can be determined by a parameter Δ',[2] which can be matched to the outer region solutions. One of the applications of Δ' is EF penetration. The calculation of Δ' is important for EF penetration and instability of tokamak plasmas. A lot of models have been developed to predict the tearing responses.[18–22] Fitzpatrick used the classic single-fluid model to map out the linear plasma response regimes in the early years.[18] Cole and Fitzpatrick use the two-fluid model to study the error field penetration,[19] which originates from the model of Hazeltine.[23] Recently, Fitzpatrick modified the drift-MHD model by considering the anomalously perpendicular particle diffusivity and obtaining the completely new two-fluid resonant layer response regimes.[17]

To realistically describe the plasma response in the inner region, the model should incorporate the plasma resistivity, $\boldsymbol{E} \times \boldsymbol{B}$ flows, electron and ion diamagnetic flows, the ion sound radius, and anomalous perpendicular transport of momentum and energy. When the magnitude of diamagnetic flows is comparable to $\boldsymbol{E} \times \boldsymbol{B}$ flows, the effect of diamagnetic flows is important. In addition, once the island width below the ion sound radius, the response of ion fluid is radically different to that of electron fluid. Moreover, it is significant to consider the realistic level of perpendicular transport of momentum and energy, because these effects obviously change the response in the inner region to error field. It is also important to calculate the screening effect of the current sheet due to the plasma flow.

2. Calculation

In this paper, we use the linearized two-fluid model[17] and the program LAYER[24] to calculate the plasma response

†Corresponding author. E-mail: xutao@hust.edu.cn

© 2024 Chinese Physical Society and IOP Publishing Ltd

in the inner region. This model includes all the above-mentioned effects. However, the formation of the layer equation is still worth a presentation for clarity. The standard cylindrical coordinates (r,θ,z) are adopted and the resonant surface is located at $r=r_{\rm s}$. The two-fluid four-field model becomes the three-field model without the parallel ion motion as[25]

$$\frac{\partial\psi}{\partial t} = [\phi,\psi]-\tau_{\rm e}[N,\psi]+\eta_{\parallel}J, \tag{1}$$

$$\frac{\partial\nabla^2\phi}{\partial t} = \left[\phi,\nabla^2\phi\right]-\frac{\tau_{\rm i}}{2}\left(\nabla^2[\phi,N]+\left[\nabla^2\phi,N\right]+\left[\nabla^2N,\phi\right]\right) +[J,\psi]+\chi_{\varphi}\nabla^4\left(\phi+\tau_{\rm i}N\right), \tag{2}$$

$$\frac{\partial N}{\partial t} = [\phi,N]+d_{\beta}^2[J,\psi]+D_{\perp}\nabla_{\perp}^2N. \tag{3}$$

Here,

$$[A,B]\equiv\nabla A\times\nabla B\cdot\boldsymbol{n},\quad \boldsymbol{n}=(0,\varepsilon/q_{\rm s},1),\quad \varepsilon=r/R_0,$$
$$\tau_{\rm e}=\tau/(1+\tau),\quad \tau_{\rm i}=1/(1+\tau),$$
$$\tau=T_{\rm e}(r_{\rm s})(1+\eta_{\rm e})/\left[T_{\rm i}(r_{\rm s})(1+\eta_{\rm i})\right].$$

$q_{\rm s}=m/n$, $\eta_{\rm e}=(\mathrm{d}\ln T_{\rm e}/\mathrm{d}\ln n_{\rm e})|_{r=r_{\rm s}}$, $\eta_{\rm i}=(\mathrm{d}\ln T_{\rm i}/\mathrm{d}\ln n_{\rm e})\big|_{r=r_{\rm s}}$, $J=\nabla^2\psi$, where $T_{\rm e}(r)$, $T_{\rm i}(r)$, and $n_{\rm e}(r)$ are electron temperature, ion temperature, and electron number density profile, respectively. Three fields are helical magnetic flux, ψ, the perturbed total plasma pressure, N, and the MHD stream function, ϕ. Moreover, $d_{\beta}=c_{\beta}d_{\rm i}$, $c_{\beta}=\sqrt{\beta/(1+\beta)}$, $\beta=(5/3)\mu_0p_{\rm s}/B_z^2$, $d_{\rm i}=\sqrt{m_{\rm i}/(n_{\rm e}e^2u_0)}$, where $p_{\rm s}$ is the total plasma pressure at resonant surface, $m_{\rm i}$, the mass of ion, e, the electrical charge. d_{β} is also referred as the ion sound radius. $\eta_{\parallel,\perp}$ is the parallel/perpendicular plasma electrical resistivity at resonant surface, χ_{φ} the anomalous perpendicular ion momentum diffusivity at the resonant surface. Finally, $D_{\perp}$ is the perpendicular particle diffusivity.

Now we assume the linear layer width is much smaller than $r_{\rm s}$. Let $x=r-r_{\rm s}$, and a perturbation $\tilde{\psi}$ takes the form $\mathrm{e}^{\mathrm{i}(\zeta-\omega t)}$, where ω is the frequency of error field, $\zeta=m\theta-nz/R_0$. Then, the background equilibrium takes the form $\psi_0(x)=x^2/2$, $\phi_0(x)=-V_{\rm E}x$, $N_0(x)=-V_*x$, where $V_{\rm E}$ is the θ component of $\boldsymbol{E}\times\boldsymbol{B}$ velocity at resonant surface, V_* the θ component of diamagnetic velocity at resonant surface. It is helpful to define the normalized variables $X=S^{1/3}x$, $Q=S^{1/3}(\omega_{\rm E}-\omega)\tau_{\rm H}$, $Q_{\rm e,i}=-S^{1/3}\omega_{*\rm e,i}\tau_{\rm H}$, $D=S^{1/3}\tau_{\rm e}^{1/2}d_{\beta}/r_{\rm s}$, $P_{\varphi}=\tau_{\rm R}/\tau_{\varphi}$, $P_{\perp}=\tau_{\rm R}/\tau_{\perp}$. Here, $S=\tau_{\rm R}/\tau_{\rm H}$ is the Lundquist number, $\tau_{\rm R}=\mu_0r_{\rm s}^2/\eta_{\parallel}$ the resistive diffusion time, $\tau_{\rm H}=L_{\rm s}/(mV_{\rm A})$ the hydromagnetic time, $\tau_{\varphi}=r_{\rm s}^2/\chi_{\varphi}$ the toroidal momentum confinement time, $\tau_{\perp}=r_{\rm s}^2/D_{\perp}$ the perpendicular particle diffusion time, $L_{\rm s}=R_0q_{\rm s}/s_{\rm s}$ the magnetic shear length, $V_{\rm A}=B_z/\sqrt{u_0n_{\rm e}(r_{\rm s})m_{\rm i}}$ the Alfvén speed, $s_{\rm s}=s(r_{\rm s})=(\mathrm{d}\ln q/\mathrm{d}\ln r)_{r_{\rm s}}$ the magnetic shear, $\omega_{\rm E}=mV_{\rm E}/r_{\rm s}$ the $\boldsymbol{E}\times\boldsymbol{B}$ frequency, $\omega_{*\rm e}=-\tau_{\rm e}(m/r_{\rm s})V_*$ the electron diamagnetic frequency, $\omega_{*\rm i}=\tau_{\rm i}(m/r_{\rm s})V_*$ the ion diamagnetic frequency. Equations (1)–(3) can be linearized for the perturbation $(\tilde{\psi},\tilde{\phi},\tilde{N})$. Retaining the first order perturbed quantities, we can obtain the linear layer equations

$$\mathrm{i}(Q-Q_{\rm e})\tilde{\psi}=\mathrm{i}X(\tilde{\phi}-\tilde{N})+\frac{\mathrm{d}^2\tilde{\psi}}{\mathrm{d}X^2}, \tag{4}$$

$$\mathrm{i}\left(Q-Q_{\rm i}\right)\frac{\mathrm{d}^2\tilde{\phi}}{\mathrm{d}X^2}=-\mathrm{i}X\frac{\mathrm{d}^2\tilde{\psi}}{\mathrm{d}X^2}+P_{\varphi}\frac{\mathrm{d}^4}{\mathrm{d}X^4}\left(\tilde{\phi}+\frac{\tilde{N}}{\tau}\right), \tag{5}$$

$$\mathrm{i}Q\tilde{N}=\mathrm{i}Q_{\rm e}\tilde{\phi}-\mathrm{i}D^2X\frac{\mathrm{d}^2\tilde{\psi}}{\mathrm{d}X^2}+P_{\perp}\frac{\mathrm{d}^2\tilde{N}}{\mathrm{d}X^2}. \tag{6}$$

Here, we make a approximation $\nabla^2\simeq\nabla_{\perp}^2\simeq S^{2/3}\mathrm{d}^2/\mathrm{d}X^2$ based on the fact $S\gg1$. Equations (4)–(6) possess independent tearing parity solutions, described by the symmetry $\tilde{\psi}(-X)=\tilde{\psi}(X)$, $\tilde{\phi}(-X)=-\tilde{\phi}(X)$, $\tilde{N}(-X)=\tilde{N}(X)$. The tearing parity solutions can be asymptotically matched to tearing-mode solutions in the outer region. We assume the asymptotic behavior of the tearing parity solutions is such that[17]

$$\tilde{\psi}\to\psi_0\left[1+\frac{\hat{\Delta}}{2}|X|+O(X^2)\right], \tag{7}$$

as $|X|\to\infty$, where ψ_0 is arbitrary constant, and $\hat{\Delta}=S^{-1/3}\Delta$. It should note that Δ parameterize the amplitude and the phase of a screening current sheet at resonant surface in response to a tearing perturbation in the outer region.

Equations (4)–(6) are conveniently solved by applying the generalized Fourier transformation, i.e., $\bar{\phi}(p)=\int_{-\infty}^{\infty}\tilde{\phi}(X)\,\mathrm{e}^{-\mathrm{i}pX}\,\mathrm{d}X$, etc. Then we get the following equations:

$$\mathrm{i}(Q-Q_{\rm e})\bar{\psi}=\frac{\mathrm{d}}{\mathrm{d}p}(\bar{\phi}-\bar{N})-p^2\bar{\psi}, \tag{8}$$

$$\mathrm{i}\left(Q-Q_{\rm i}\right)p^2\bar{\phi}=\frac{\mathrm{d}(p^2\bar{\psi})}{\mathrm{d}p}-P_{\varphi}p^4\left(\bar{\phi}+\frac{\bar{N}}{\tau}\right), \tag{9}$$

$$\mathrm{i}Q\bar{N}=\mathrm{i}Q_{\rm e}\bar{\phi}-D^2\frac{\mathrm{d}(p^2\bar{\psi})}{\mathrm{d}p}-P_{\perp}p^2\bar{N}, \tag{10}$$

where a tearing parity solution satisfies $\bar{\phi}(p)\to\bar{\phi}_0[1+\hat{\Delta}/(\pi p)+\mathcal{O}(p)]$, as $p\to0$.

Finally, Let us rearrange Eqs. (8)–(10) by eliminating $\bar{\phi}$ and define $Y_{\rm e}=\bar{\phi}-\bar{N}$, then we get the linear layer equation[17]

$$\frac{\mathrm{d}}{\mathrm{d}p}\left[\frac{p^2}{\mathrm{i}(Q-Q_{\rm e})+p^2}\frac{\mathrm{d}Y_{\rm e}}{\mathrm{d}p}\right]-\frac{A(p)}{B(p)}p^2Y_{\rm e}=0, \tag{11}$$

with

$$A(p) = -Q\left(Q-Q_{\rm i}\right)+\mathrm{i}\left(Q-Q_{\rm i}\right)\left(P_{\varphi}+P_{\perp}\right)p^2 +P_{\varphi}P_{\perp}p^4, \tag{12}$$

$$B(p) = \mathrm{i}(Q-Q_{\rm e})+\left[P_{\perp}+\mathrm{i}\left(Q-Q_{\rm i}\right)D^2\right]p^2 +(1+1/\tau)P_{\varphi}D^2p^4. \tag{13}$$

The boundary conditions of $Y_{\rm e}(p)$ are $\lim\limits_{p\to+\infty}Y_{\rm e}(p)=0$ and

$$\lim_{p\to+0}Y_{\rm e}(p)=Y_0\left[1+\hat{\Delta}/(\pi p)+\mathcal{O}(p)\right]. \tag{14}$$

Equation (11) can be solved numerically with good accuracy by using the Riccati transformation[25] to obtain $\hat{\Delta}$.

$\hat{\Delta}(Q,Q_e,Q_i,D,P_\varphi,P_\perp)$ is a critical parameter because the plasma response to error field in the inner region is characterized by this parameter. As is shown, $\hat{\Delta}$ is the function of six normalized parameters. We assume the error field is static (i.e., $\omega=0$) in this study. The effects of the $\boldsymbol{E}\times\boldsymbol{B}$ frequency, the electron diamagnetic frequency, the ion diamagnetic frequency, the ion sound radius, anomalous perpendicular momentum and energy transport are parameterized by Q, Q_e, Q_i, D, P_φ, and $P_\perp$, respectively.

The second work is the calculation of the plasma response in the outer region. The system is assumed to be periodic in toroidal direction with the periodicity $2\pi R_0$, where R_0 is the major radius of the plasma. Let a be the minor radius of the plasma. A large aspect ratio tokamak plasma is adopted, which implies $a/R_0 \ll 1$. The equilibrium magnetic field is $\boldsymbol{B}=[0,B_\theta(r),B_z]$, where $B_\theta(r)$ is the poloidal magnetic field-strength and B_z is the spatially uniform toroidal magnetic field-strength. The equilibrium plasma current density is written as $\boldsymbol{j}=[0,0,j_z(r)]$, and the safety-factor is $q(r)=rB_z/(R_0B_\theta)$. In the outer region, the plasma response to error field is calculated from the cylindrical tearing mode equation.[26] For simplicity, we assume the plasma is surrounded by a rigid, perfectly conducting and concentric wall at $r=r_w$ $(r_w>a)$. The perturbed helical magnetic flux in the outer region can be written as $\delta\psi(r,\theta,z)=\delta\psi(r)\,e^{i(m\theta-nz/R_0)}$, and $\delta\psi(r)$ satisfies the cylindrical tearing mode equation

$$\frac{\partial^2\delta\psi}{\partial r^2}+\frac{1}{r}\frac{\partial\delta\psi}{\partial r}-\frac{m^2}{r^2}\delta\psi-\frac{J_z'\delta\psi}{r(1/q-n/m)}=0, \tag{15}$$

where $J_z'=\mathrm{d}J_z/\mathrm{d}r$ and $J_z(r)=R_0\mu_0 j_z(r)/B_z$. The solution of Eq. (15) is continuous across resonant surface, but its gradient to minor radius is discontinuous across the surface due to the presence of inductive current sheet at the surface. Let the complex quantity $\Psi_s=\delta\psi(r_s)$ denote the amplitude and the phase of the reconnected magnetic flux at $r=r_s$, and the quantity $\Psi_w=\delta\psi(r_w)$ specifies the amplitude and phase of flux of the error field at $r=r_w$. $\delta\psi(r)$ takes the form $\delta\psi(r)=\Psi_s\hat{\psi}_s(r)+\Psi_w\hat{\psi}_w(r)$, where $\hat{\psi}_s(r)$ is a real solution of Eq. (15) which satisfies $\hat{\psi}_s(0)=0$, $\hat{\psi}_s(r_s)=1$, and $\hat{\psi}_s(r\geq r_w)=0$. In addition, $\hat{\psi}_w(r)$ satisfies $\hat{\psi}_w(r\leq r_s)=0$, $\hat{\psi}_w(r_w)=1$. The tearing eigenfunctions $\hat{\psi}_s(r)$, $\hat{\psi}_w(r)$ can be solved by using the method of Ref. [27].

The solution of Eq. (15) can asymptotically match to the solution in the inner region, which yields[26]

$$\left[r\frac{\partial\delta\psi}{\partial r}\right]_{r=r_{s-}}^{r=r_{s+}}=\Delta\Psi_s=E_{ss}\Psi_s+E_{sw}\Psi_w. \tag{16}$$

Here, $E_{ss}=[r\mathrm{d}\hat{\psi}_s/\mathrm{d}r]_{r=r_{s-}}^{r=r_{s+}}$ is the conventional stability index,[2] and $E_{sw}=[r\mathrm{d}\hat{\psi}_w/\mathrm{d}r]_{r=r_s}$. Then, the reconnected magnetic flux (considering the plasma response) is

$$\Psi_s=\frac{E_{sw}}{\Delta-E_{ss}}\Psi_w. \tag{17}$$

Then, the reconnection magnetic flux in the absence of plasma response is $\Psi_v=-E_{sw}\Psi_w/E_{ss}$.

Let us define the screening factor Σ that represents the ratio of amplitude of the reconnected magnetic flux in the absence and in the presence of shielding current. The screening factor can be written as

$$\Sigma=\frac{|\Psi_v|}{|\Psi_s|}=\frac{|\Delta-E_{ss}|}{-E_{ss}}. \tag{18}$$

In fact, $\Sigma=\Sigma(Q)$ is the function of $\boldsymbol{E}\times\boldsymbol{B}$ rotation. Normalizing the variables in the right-hand of Eq. (18) by multiplying $S^{-1/3}$, we get

$$\Sigma(Q)=\frac{\left(\left[\zeta+\hat{\Delta}_r(Q)\right]^2+\left[\hat{\Delta}_i(Q)\right]\right)^{1/2}}{\zeta}, \tag{19}$$

where $\zeta=S^{-1/3}(-E_{ss})$, $\hat{\Delta}_r(Q)$ is the real part of $\hat{\Delta}(Q)$, $\hat{\Delta}_i(Q)$ is the imaginary part of $\hat{\Delta}(Q)$.

Substituting the radial magnetic field-strength $b_r=r_s\Psi_s/m$ into Eq. (17) and setting $\Sigma=1$, we can obtain

$$\frac{b_v}{B_z}=\frac{mR_0}{r_s}\frac{E_{sw}}{(-E_{ss})}\left|\hat{\Psi}_w\right|, \tag{20}$$

where b_v is the radial perturbed magnetic field-strength in the absence of the plasma response at the resonant surface, and $\hat{\Psi}_w=\Psi_w/R_0B_z$.

The width of island chain driven at the resonant surface is

$$W=4\left(\frac{1}{ns_s\varepsilon_s}\frac{b_v}{B_z}\frac{1}{\Sigma}\right)^{1/2}r_s, \tag{21}$$

where use has been made of Eqs. (17)–(20) and $W=4\left(L_sR_0\left|\hat{\Psi}_s\right|\right)^{1/2}$.

The final task is the calculation of torque balance equation to obtain the penetration threshold of error field. We assume that the electron and ion diamagnetic frequency keep unchanged after applying error field, and $\boldsymbol{E}\times\boldsymbol{B}$ velocity profile can be modified by the electromagnetic torque. Then, the torque balance equation is[28]

$$\frac{\mathrm{Im}\left[\hat{\Delta}(Q)\right]\bar{I}_c^2}{|\zeta+\hat{\Delta}(Q)|^2}=Q_{E0}-Q, \tag{22}$$

where $Q_{E0}=S^{-1/3}\omega_{E0}\tau_H$, and ω_{E0} is the $\boldsymbol{E}\times\boldsymbol{B}$ frequency in the absence of error field. Moreover,

$$\bar{I}_c=\frac{1}{2\varepsilon_sS_s}\left[\left(\frac{q_s}{\varepsilon_s}\right)^2\left(\frac{\tau_\theta}{\tau_\varphi}\right)^{1/2}+2\ln\left(\frac{a}{r_s}\right)\right]^{1/2}\times\left(\frac{S}{P_\varphi}\right)^{1/2}E_{sw}|\hat{\Psi}_w|. \tag{23}$$

Here, τ_θ is the ion poloidal flow-damping timescale at $r=r_s$. The left-hand term of Eq. (22) denotes the electromagnetic braking torque at the resonant surface, and the right-hand term

of Eq. (22) represents the viscous torque. Equation (22) also can be written as $\bar{I}_c^2 = F(Q)$, where

$$F(Q) = (Q_{E0} - Q)\frac{|\zeta + \hat{\Delta}(Q)|^2}{\mathrm{Im}\left[\hat{\Delta}(Q)\right]}. \tag{24}$$

Let $\bar{I}_{cp}$ be the critical value of normalized coil current to trigger penetration. $\bar{I}_{cp}$ can be calculated from Eq. (22). Then, the penetration threshold of the error field is

$$\left(\frac{b_v}{B_z}\right)_{pene} = \frac{2ms_s}{(-E_{ss})}\left[\left(\frac{q_s}{\varepsilon_s}\right)^2\left(\frac{\tau_\theta}{\tau_\varphi}\right)^{1/2} + 2\ln\left(\frac{a}{r_s}\right)\right]^{-1/2} \times \left(\frac{P_\varphi}{S}\right)^{1/2}\bar{I}_{cp}, \tag{25}$$

where use has been made of Eqs. (20), (22), and (23).

A "Wesson"-type safety factor profile[29] is used in the simulation. Let q_a be the safety factor at plasma boundary, and q_0 is the safety factor at magnetic axis. The equilibrium electron temperature profile of $T_e(r) = T_{e0}\left(1 - r^2/a^2\right)^{\nu_1}$, is introduced, where T_{e0} is the electron temperature of the plasma core, ν_1 the shape factor. Additionally, the density profile is $n_e(r) = n_{e0}\left(1 - r^2/a^2\right)^{\nu_2}$, where n_{e0} is the electron number density of the plasma core, ν_2 the shape factor. We assume the ion temperature profile, $T_i(r)$ possesses the same shape of $T_e(r)$, but the core ion temperature, T_{i0}.

Consider the response of a J-TEXT plasma, Shot No. 1042126, to a 2/1 tearing mode.[7] The input parameters in the simulation are based on the parameter of this shot. The parameters are $a = 0.255$ m, $R_0 = 1.05$ m, $I_p = 160$ kA, $B_z = 1.8$ T, $T_{e,q=2} = 250$ eV, $T_{i,q=2} = 180$ eV, $n_{e,q=2} = 0.4 \times 10^{19}$ m^{-3}, $\omega_{*e} = 2\pi \times 2$ krad/s, $\omega_{E0} = 2\pi \times 6$ krad/s, $\nu_1 = 2.8$, $\nu_2 = 1.3$, $\chi_\varphi = 0.5$ m^2/s, $D_\perp = 0.3$ m^2/s, $q_a = 3.4$, $q_0 = 0.56$, $r_s = 0.77a$, $r_w = 1.18a$. Note that ν_1 and ν_2 are obtained by fitting the experimental data. Finally, we can obtain normalized parameters $Q_e = -6.83 \times 10^{-2}$, $Q_i = 4.92 \times 10^{-2}$, $Q_{E0} = 0.215$, $D = 1.18$, $P_\varphi = 2.80$, $P_\perp = 1.27$.

3. Results

The complex layer-matching index $\hat{\Delta}$ which parameterizes the plasma response to error field in the inner region is shown in Fig. 1. The imaginary part of $\hat{\Delta}$ monotonically increases with the normalized $\boldsymbol{E} \times \boldsymbol{B}$ frequency Q, and the real part of $\hat{\Delta}$ approaches to 0 in a wide range of Q. So, the phase of $\hat{\Delta}$ is close to $\pi/2$. It should be noted that the response of the viscous-resistive (VR) regime and the diffusive-resistive (DR) regime are purely imaginary.[17,18] In addition, the plasma response vanishes (i.e., $\hat{\Delta} = 0$) at $Q = Q_e$, where the electron fluid is static. The response on the initial $\boldsymbol{E} \times \boldsymbol{B}$ frequency of Shot No. 1042126 corresponds to the solid dot in Fig. 1. The magnetic Prandtl number is estimated by $P \simeq \sqrt{P_\varphi P_\perp} \simeq 1.89$. The normalized parameters satisfy $D^6 = 2.70 > P$, $D^2 Q_{E0}^{-2} = 30.12 > P$, $Q_{E0}^2 D^{-2} = 0.03 < P$. Thus, we deduce that the response in the shot lies in the DR regime according to Ref. [17]. The response in the DR regime is dominated by the perpendicular particle diffusion and plasma resistivity. According to the Fitzpatrick's theory, the nonlinear response regime bifurcates to seven regimes, including Rutherford regime, Waelbroeck regime, and so on,[18] which is also calculated by Wang *et al.*[30]

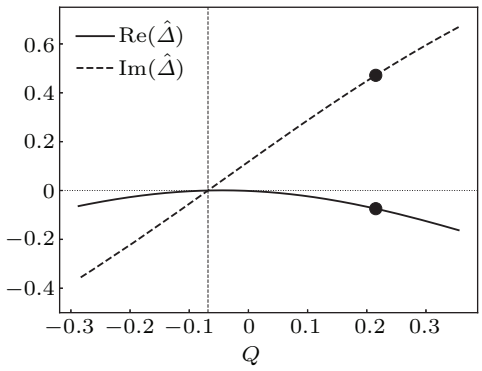


Fig. 1. Complex layer-matching parameter $\hat{\Delta}$, which characterizes the plasma response to error field in the inner region, is the function of normalized $\boldsymbol{E} \times \boldsymbol{B}$ frequency Q. Re denotes the real part, and Im denotes the imaginary part. Here, the five parameters are $(Q_e, Q_i, D, P_\varphi, P_\perp) = (-6.83 \times 10^{-2}, 4.92 \times 10^{-2}, 1.18, 2.80, 1.27)$. The vertical dashed line corresponds to $Q = Q_e$, and the solid dot shows the $\hat{\Delta}(Q_{E0})$, $Q_{E0} = 0.215$.

The screening factor as a function of the normalized $\boldsymbol{E} \times \boldsymbol{B}$ frequency is shown in Fig. 2. The solid dot indicates the strong screening effect of plasma rotation before applying the error field. The screening factor increases almost linearly with $|Q - Q_e|$ (i.e., the perpendicular electron frequency). After penetration, the mode is locked to the error field and the mode frequency approaches to 0 ($Q \approx Q_e$). There is no inductive current at the rational surface to shield the radial perturbed field. Thus, the perturbed radial magnetic field is nearly equal to the vacuum radial magnetic field at the rational surface (i.e., $\Sigma \approx 1$).

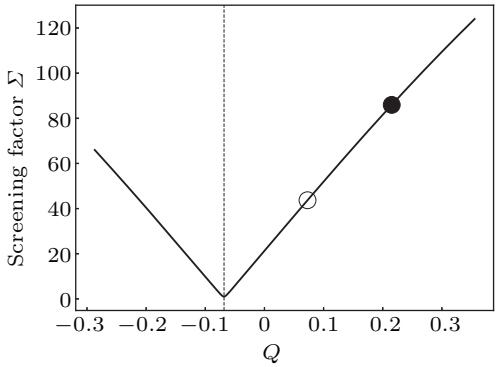


Fig. 2. The screening factor, $\Sigma(Q)$ of shot No. 1042126 with parameters $(Q_e, Q_i, D, P_\varphi, P_\perp) = (-6.83 \times 10^{-2}, 4.92 \times 10^{-2}, 1.18, 2.80, 1.27)$, and $\zeta = 5.54 \times 10^{-3}$. The vertical dashed line corresponds to $Q = Q_e$. The solid dot shows the $\Sigma = 86$, at the initial $\boldsymbol{E} \times \boldsymbol{B}$ frequency $Q_{E0} = 0.215$ and the vacuum dot shows $\Sigma = 43.7$ at the critical point just before penetration.

The normalized tearing eigenfunctions $\hat{\psi}_s(r)$ and $\hat{\psi}_w(r)$ that denote the tearing-stable plasma response to error field in the outer region is shown in Fig. 3, with $E_{ss} = -1.1$, $E_{sw} = 2.0$.

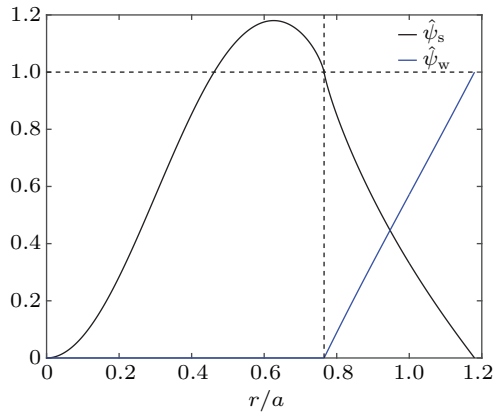


Fig. 3. Normalized tearing eigenfunctions calculated for J-TEXT plasma of shot No. 1042126. The vertical dashed line shows the location of 2/1 rational surface.

The solutions of torque balance equation are shown in Fig. 4. The natural mode frequency (the unperturbed electron fluid rotation frequency) takes the form $\omega_{\perp e0} = \omega_{E0} + \omega_{*e}$, which is determined by the sum of the electron diamagnetic frequency and initial $\boldsymbol{E} \times \boldsymbol{B}$ frequency.[19] There are three branches: A–B, B–C, and C–D. When the amplitude of error field is increased from zero, Q will follow the high-slip branch that starts from A to B. On this branch, $\omega_{\perp e} \gg 0$ and the magnetic reconnection is strongly suppressed by the plasma rotation. Once $\omega_{\perp e}$ reaches point B, the bifurcation will occur and $\omega_{\perp e}$ jumps to low-slip branch C–D. On this branch, $\omega_{\perp e} \approx 0$ and the electron fluid is suddenly arrested by error field. Thus, the shielding current vanishes and the magnetic reconnection grows unhindered. It is noted that the solution of branch B–C is dynamically unstable.[31] It never be accessed on realistic condition.

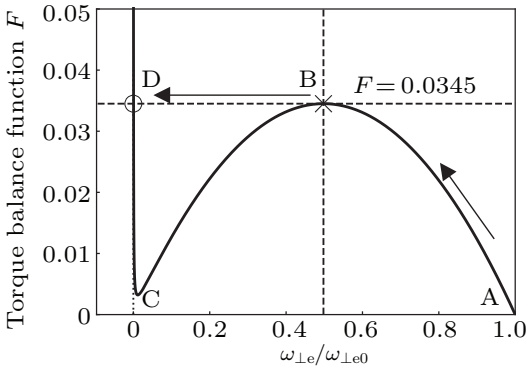


Fig. 4. Torque balance curve $\bar{I}_c^2 = F(\omega_{\perp e})$ for shot No. 1042126 with parameters $(Q_e, Q_i, D, P_\varphi, P_\perp) = (-6.83 \times 10^{-2}, 4.92 \times 10^{-2}, 1.18, 2.80, 1.27)$, $\zeta = 5.54 \times 10^{-3}$, and $Q_{E0} = 0.215$. Here, $\bar{I}_c$ is the normalized coil current, $\omega_{\perp e}$ the perpendicular electron frequency. The critical value of normalized coil current to trigger penetration corresponds to $F = \bar{I}_c^2 = \bar{I}_{cp}^2$. The vertical dashed line denotes the $\boldsymbol{E} \times \boldsymbol{B}$ frequency just before the penetration.

The saturated island width varies with the amplitude of the error field in Fig. 5. As the amplitude increases, the saturated island width increases slowly, and the island width is very small. In this stage, the magnetic reconnection is suppressed strongly by the plasma rotation. Once the amplitude is above a threshold value, the saturated island width jumps to a very large size. In addition, if we continue increasing the amplitude of the error field, the saturated island rises rapidly relative to its size before penetration. A large size island can lead to plasma disruption. The critical value radial error field at the 2/1 rational surface is 9.7 Gs (1 Gs = 10^{-4} T) in simulation, and the penetration threshold of radial 2/1 component of resonant magnetic field at the resonant surface employed to the shot No. 1042126 is 8.7 Gs. The simulation results are in good agreement with the experimental results.

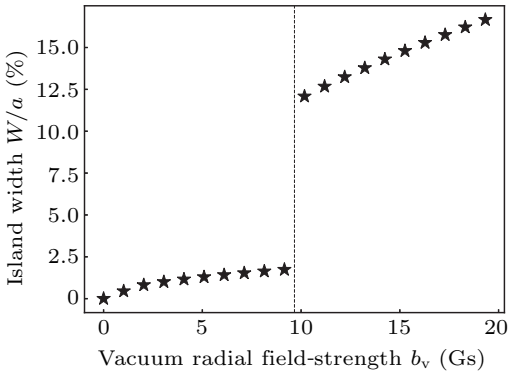


Fig. 5. The 2/1 island width versus the vacuum radial magnetic field-strength at the 2/1 surface with parameters $(Q_e, Q_i, D, P_\varphi, P_\perp) = (-6.83 \times 10^{-2}, 4.92 \times 10^{-2}, 1.18, 2.80, 1.27)$. The vertical dashed line corresponds to the penetration threshold of $b_v = 9.7$ Gs.

We scan the natural mode frequency while the electron diamagnetic frequency $\omega_{*e} = 2\pi \times 2$ kHz keeps unchanged. Figure 6(a) shows the critical radial field to trigger penetration linearly increases with $|\omega_{\perp e0}|$. Actually, the penetration threshold between the positive and negative natural frequencies is not completely symmetric. According to Fitzpatrick's simulation in ITER and SPARC, the ohmically heated plasma is more susceptible to penetration when the electron fluid at resonant surface rotates in the ion diamagnetic direction, rather than in the electron diamagnetic direction.[27] Recently, an experiment on the mode penetration with the NBI in EAST has been conducted.[32]

When the natural mode frequency is close to zero, the penetration threshold of the error field cannot reach zero, and the bifurcation phenomenon disappear. The experimental results in TEXTOR show that penetration threshold reaches a minimum value when the frequency of the external field is equal to the mode frequency.[33] To avoid the disappearance of the bifurcation, we artificially set the mode frequency reduce to 5% of its initial value when the natural mode frequency approaches to zero. In addition, when the level of natural mode frequency is much larger than diamagnetic frequency, $(b_v/B_z)_{pene}$ keeps well above 10^{-4}. Figure 6(b) shows the ratio of electron fluid frequency to natural frequency versus the natural frequency before and after penetrations. When $|\omega_{\perp e0}|$ is much larger than electron diamagnetic frequency, $\omega_{\perp e}/\omega_{\perp e0} \approx 0.5$ before penetration. However, the electron

fluid frequency is reduced to zero after penetration. When $|\omega_{\perp e0}|$ is less than electron diamagnetic frequency, $\omega_{\perp e}/\omega_{\perp e0}$ decreases with $|\omega_{\perp e0}|$ before penetration, and slightly increases with $|\omega_{\perp e0}|$ after penetration. Figure 6(c) shows the saturated island width very small ($W/a < 2\%$) before penetration. After penetration, the saturated island width increases rapidly with natural frequency, and the island width is much larger than the width before penetration. In addition, the W/a will exceed 10%, if $|\omega_{\perp e0}/\omega_{*e}| > 3$. Finally, figure 6(d) shows the screening factor rises linearly with natural frequency before penetration. It should be noted that when the natural frequency approaches zero, the shielding effect is very weak. After penetration, the screening effect completely vanishes, so the screening factor falls to the unit.

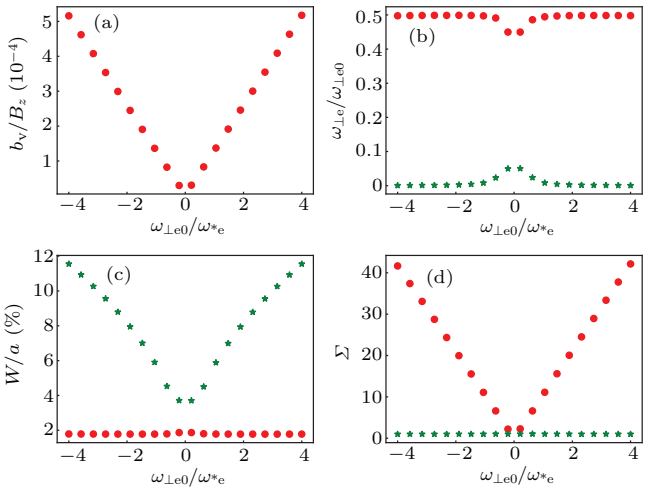


Fig. 6. Error field penetration threshold versus natural mode frequency $\omega_{\perp e0}$ in J-TEXT. (a) The threshold of the radial field as a function of natural mode frequency. (b) The perpendicular electron frequency before (dot) and after penetration (star). (c) The island width before (dot) and after penetration (star). (d) The screening factor before (dot) and after penetration (star).

The effect of electron temperature at $m/n = 2/1$ surface for the penetration threshold of J-TEXT can be studied by scanning $T_{e,q=2}$ from 50 eV to 450 eV as shown in Fig. 7. For the simplicity, ω_{*e} is artificially kept unchanged while scanning $T_{e,q=2}$. Other parameters are $T_{i,q=2} = 0.1$ keV, $n_{e,q=2} = 0.6 \times 10^{19}$ m^{-3}, $B_z = 1.8$ T, $\omega_{*e} = 2\pi \times 2$ krad/s, $\chi_\varphi = 0.5$ m^2/s, $D_\perp = 0.3$ m^2/s. The threshold (green squares) increases with the increasing $T_{e,q=2}$, and a least-squares fitting is applied as shown by the green curve, which indicates $b_v/B_z \propto T_e^{0.54}$. The scaling reveals the positive dependence on electron temperature.

In addition, the effect of electron number density at $m/n = 2/1$ surface for the penetration threshold can be studied by scanning $n_{e,q=2}$ from 0.2×10^{19} m^{-3} to 2.0×10^{19} m^{-3} as shown in Fig. 8. Other parameters are $T_{e,q=2} = T_{i,q=2} = 0.1$ keV, $B_z = 1.8$ T, $\omega_{*e} = 2\pi \times 2$ krad/s, $\chi_\varphi = 0.5$ m^2/s, $D_\perp = 0.3$ m^2/s. The electron density scaling is $b_v/B_z \propto n_e^{0.75}$, which is obtained by least-squares fitting. The scaling is stronger than the experiment scaling $\alpha_n \sim 0.5$ observed in J-TEXT.[9] The possible reason is the finite diamagnetic frequency and the ion sound radius effect in the model. In temperature scanning, we regard the electron temperature as independent quantity. In fact, temperature varies with electron density. The experimental scaling of J-TEXT is $T_e \propto n_e^{-0.63}$.[10] Thus, the penetration scaling is $b_v/B_z \propto n_e^{0.41}$, if the density dependence of the electron temperature takes into consideration.

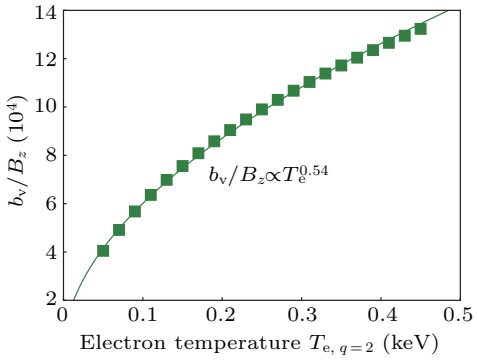


Fig. 7. The dependence of EF penetration threshold on $m/n = 2/1$ error field penetration threshold versus electron temperature at $q = 2/1$ surface. The penetration scaling obtained by least-squares fitting for numerical results is $b_v/B_z \propto T_e^{0.54}$ for $\omega_{\perp e0} = 4\omega_{*e}$.

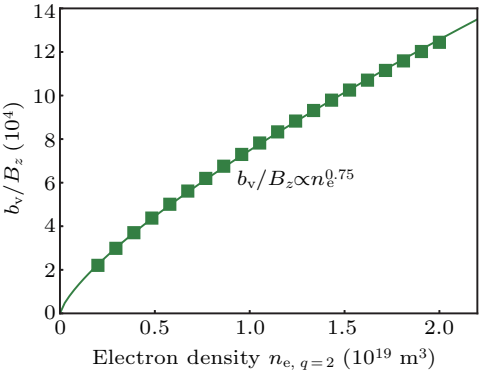


Fig. 8. The dependence of EF penetration threshold on $m/n = 2/1$ error field penetration threshold versus electron number density at $q = 2/1$ surface. The penetration scaling obtained by least-squares fitting for numerical results is $b_v/B_z \propto n_e^{0.75}$ for $\omega_{\perp e0} = 4\omega_{*e}$.

4. Conclusion

We calculated the plasma response of J-TEXT to error field in the inner region by using the two-fluid model. The model considers diamagnetic magnetic drift, $\boldsymbol{E} \times \boldsymbol{B}$ flow, ion sound radius, and anomalous perpendicular energy, and momentum transport. By solving the cylindrical tearing mode equation, we can obtain the plasma response in the outer regions, and then the asymptotic matching between the inner and outer region allows us to calculate the 2/1 error field penetration threshold.

We then illustrated the physical process of error field penetration in Fig. 4, where the mode frequency jumps from a finite value to 0 when the error field amplitude is larger than a critical value. In order to characterize the shielding effect of the induced current at the resonance surface on the error field,

we introduced the shielding factor. The shielding effect of the plasma on the error field disappears completely when the mode frequency approaches zero. Similarly, there is a jump in the saturated magnetic island width before and after field penetrations, with a significant increase in the island width after penetration and a strong suppression of magnetic reconnection before penetration.

Moreover, we scanned the natural mode frequency and found that the shielding of the error field by the plasma decreases as the natural mode frequency decreases and that $\omega_{\perp e}/\omega_{\perp e0}$ decreases slightly as the natural mode frequency approaches zero. Then, we scanned the electron temperature and density separately and obtained the penetration scaling of $b_v/B_z \propto n_e^{0.75} T_e^{0.54}$. Finally, we considered the experimental relation $T_e \propto n_e^{-0.63}$, the scaling is modified as $b_v/B_z \propto n_e^{0.41}$.

Data availability statement

The data that support the findings of the present study are openly available in the Science Data Bank at https://doi.org/10.57760/sciencedb.j00113.00200.

Acknowledgements

The authors are grateful for help of J-TEXT team. The authors are grateful to Professor R. Fitzpatrick for helpful suggestions and the support of program LAYER. Project supported by the National Natural Science Foundation of China (Grant No. 51821005).

References

[1] Sweet P 1958 *Il Nuovo Cimento* **8** 188
[2] Furth H P, Killeen J and Rosenbluth M N 1963 *Phys. Fluids* **6** 459
[3] Parker E N 1963 *Astrophys. J. Suppl. Ser.* **8** 177
[4] Hender T, Fitzpatrick R, Morris A, Carolan P, Durst R, Edlington T, Ferreira J, Fielding S, Haynes P and Hugill J 1992 *Nucl. Fusion* **32** 2091
[5] Scoville J, La Haye R, Kellman A, Osborne T, Stambaugh R, Strait E and Taylor T 1991 *Nucl. Fusion* **31** 875
[6] Buttery R, De'Benedetti M, Gates D A, Gribov Y, Hender T, La Haye R, Leahy P, Leuer J, Morris A and Santagiustina A 1999 *Nucl. Fusion* **39** 1827
[7] Yan W, Chen Z Y, Huang D W, Hu Q M, Shi Y J, Ding Y H, Cheng Z F, Yang Z J, Pan X M, Lee S G, Tong R H, Wei Y N, Dong Y B and the J-TEXT Team 2018 *Plasma Phys. Controlled Fusion* **60** 035007
[8] Wang N, Ding Y, Rao B and Li D 2022 *Rev. Mod. Plasma Phys.* **6** 26
[9] Wang N, Rao B, Hu Q, Ding Y, Chen Z, Gao L, Jin W, Yi B, Zeng W and Li Q 2014 *Nucl. Fusion* **54** 064014
[10] Huang Z, Liang Y, Hu Q, Wang N, Li D, Zhang X, Rao B, Chen Z, Zhou S, Zhang Q, Shen C, He Y, Ding Y and the J-TEXT Team 2020 *Nucl. Fusion* **60** 064003
[11] Wang N, Liang Y, Ding Y, Chen Z, Chen Z, Yang Z, Xia D, Zheng W, Yan W and Li D 2022 *Nucl. Fusion* **62** 042016
[12] Fitzpatrick R 2012 *Plasma Phys. Controlled Fusion* **54** 094002
[13] Wolf R, Biel W, De Bock M, Finken K, Günter S, Hogeweij G, Jachmich S, Jakubowski M, Jaspers R and Krämer-Flecken A 2005 *Nucl. Fusion* **45** 1700
[14] Howell D, Hender T and Cunningham G 2007 *Nucl. Fusion* **47** 1336
[15] Park J K, Menard J E, Gerhardt S P, Buttery R J, Sabbagh S A, Bell R E and LeBlanc B P 2012 *Nucl. Fusion* **52** 023004
[16] Wang H H, Sun Y W, Shi T H, Zang Q, Liu Y Q, Yang X, Gu S, He K Y, Gu X and Qian J P 2018 *Nucl. Fusion* **58** 056024
[17] Fitzpatrick R 2022 *Phys. Plasmas* **29** 032507
[18] Fitzpatrick R 1998 *Phys. Plasmas* **5** 3325
[19] Cole A and Fitzpatrick R 2006 *Phys. Plasmas* **13** 032503
[20] Waelbroeck F 2003 *Phys. Plasmas* **10** 4040
[21] Waelbroeck F, Joseph I, Nardon E, Bécoulet M and Fitzpatrick R 2012 *Nucl. Fusion* **52** 074004
[22] Militello F and Waelbroeck F 2009 *Nucl. Fusion* **49** 065018
[23] Hazeltine R, Kotschenreuther M and Morrison P 1985 *Phys. Fluids* **28** 2466
[24] Fitzpatrick R https://github.com/rfitzp
[25] Park J K 2022 *Phys. Plasmas* **29** 072506
[26] Fitzpatrick R 1993 *Nucl. Fusion* **33** 1049
[27] Fitzpatrick R 2023 *Phys. Plasmas* **30** 092512
[28] Fitzpatrick R 2023 *Tearing mode dynamics in tokamak plasmas* (IOP Publishing) pp. 177–179
[29] Wesson J 1978 *Nucl. Fusion* **18** 87
[30] Wang H, Wang Z, Ding Y and Rao B 2015 *Plasma Sci. Technol.* **17** 539
[31] De Bock M, Classen I, Busch C, Jaspers R, Koslowski H, Unterberg B and the TEXTOR Team 2008 *Nucl. Fusion* **48** 015007
[32] Ye C, Sun Y W, Wang H H, Liu Y Q, Shi T H, Li Y Y, Zang Q, Lu D A, Jia T Q and Ma Q 2023 *Nucl. Fusion* **64** 016005
[33] Koslowski H, Liang Y, Krämer-Flecken A, Löwenbrück K, Von Hellermann M, Westerhof E, Wolf R, Zimmermann O and the TEXTOR Team 2006 *Nucl. Fusion* **46** L1